

# Pixel analysis of a force-sensing device based on individually contacted vertical piezoelectric nanowires

Edgar A. A. Leon Perez, Emmanuelle Pauliac-Vaujour  
CEA-LETI  
F-38054 Grenoble, France  
[edgar.leonperez@cea.fr](mailto:edgar.leonperez@cea.fr)

Mireille Mouis  
CNRS, IMEP-LAHC, F-38000 Grenoble, France  
Univ. Grenoble Alpes, IMEP-LAHC  
F-38000 Grenoble, France

**Abstract**—We report on the static finite element (FEM) simulations of the representative pixel of a force-sensing device, with the aim of predicting the influence of technically tunable parameters on pixel response. This pixel was based on an individually contacted vertical nanowire. It was found that piezopotential collection efficiency was higher for thinner seed-layers, reaching up to 69 % for a 5 nm-thick layer. The degradation resulting from a gap between the NW and its contacts was quantified, lowering this value to 33 % for a 3 nm gap. The values chosen for technological parameters were based on experimental results and set to a range of plausible values for selective growth of ZnO nanowires on pre-patterned substrates. Our results provide important guidelines for the optimization of sensor pixel piezoelectric response, with resulting constraints on NW growth and substrate patterning.

**Keywords**—Nanosensors, simulation, ZnO Nanowire, piezoelectricity

## I. INTRODUCTION

One-dimensional nanostructures exhibit high elasticity [1]. Piezoelectric nanowires (NWs), such as GaN or ZnO NWs, have focused attention because of their potential applications in nanoelectronic devices [2]. The interest of vertical piezoelectric NWs for high sensitivity sensors applications has already been investigated [3].

In this work, we simulate a force-displacement sensor based on a matrix of pixels made of individually contacted vertical piezoelectric NWs. The theoretical analysis of a single NW has been reported in [4], where a model of the piezopotential response under bending has been developed and validated. The impact of electrical contacts size and position has already been investigated in [5] for a single NW, although technological issues and device feasibility were not addressed.

Our aim with these simulations is to gain in-depth understanding of the pixel piezoelectric behavior in view of system integration. For this purpose, a certain number of practical issues must be addressed. Here, we assumed that growth parameters can be controlled independently and we concentrated on pixel architecture and process related parameters, with account to their potential variability.

Our approach is original in that it accounts for the surrounding environment of the NW, with realistic geometrical

parameters that correspond to technologically plausible conditions. In particular, we analyzed the pixel response as a function of seed-layer thickness, electrodes distance to the NW and electrodes thickness. This analysis was carried out using multi-physics simulations based on the finite element method (FEM). It provides guidelines to improve device sensitivity.

## II. DEVICE CONCEPT

### A. Pixel description and boundary conditions

The device pixel considered in this work was made up of a silicon substrate, a ZnO seed-layer, one vertical ZnO NW and two gold metallic electrodes placed at the NW base. The NW is modeled as a cylinder with a length of 600 nm and a diameter of 50 nm (Fig. 1). FEM calculations were performed with COMSOL Multiphysics software.

The working principle of the pixel is based on the collection of charges generated at the bottom region of the NW upon bending. This region, often called the piezopotential inversion region, hosts the highest piezopotential values for the configuration under study. With ZnO NWs, which are semi-conducting, the generated piezopotential can be exploited to tune the I-V characteristics as a function of strain-stress state, due to the Schottky nature of the metal-semiconductor contacts. This is the so-called piezotronic effect, which results from a strain-induced variation of Schottky barrier height [6].

The ZnO NW and seed-layer were considered to behave like purely piezoelectric materials. This approximation assumes that the doping level is low enough to allow free charge effects to be neglected. It is beyond the scope of present paper to account for free charges and dynamic effects and this will not be discussed further here.

The pixel was considered to be integrated on a silicon substrate. The width at the base was fixed to 200 nm. The electrode from the side where the force is applied was grounded, while the other one was considered to be at a floating potential. A lateral force  $F$  was applied to a 5-nm-high shell element at the upper free end of the NW. The force was thus distributed on a quarter-circular surface of 98 nm<sup>2</sup>. The force was kept below  $F = 80$  nN. This maximum value resulted in a 124 nm deflection of the free-end of the NW, which was assumed to be the limit of the linear mechanics regime [7].

Additionally, we used bulk values for the linear elastic coefficients (stiffness and compliance) and for the piezoelectric coefficients of ZnO.

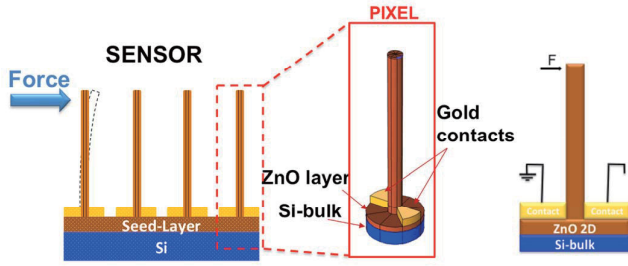


Fig. 1. Schematics of the force-displacement sensing device pixel based on a vertical piezoelectric nanowire.

### B. Theoretical frame

In a piezoelectric material, mechanical and electrical behaviors are coupled by the following equations:

$$[D]=[e]^T[S]+[\epsilon][E] \quad (1)$$

$$[T]=[c][S]-[\epsilon][E] \quad (2)$$

where  $[D]$  is the electric displacement field vector,  $[S]$  and  $[T]$  are the strain and stress tensors, respectively,  $[E]$  is the electric field vector,  $[e]$ ,  $[\epsilon]$  and  $[c]$  stand for the linear piezoelectric, the dielectric and stiffness tensors respectively. Equation (1) describes the direct piezoelectric effect, i.e. the polarization produced by mechanical strain, whereas (2) describes the converse piezoelectric effect, i.e. mechanical strain produced by an electric field.

Wang *et al.* first proposed a continuum model describing the electrostatic potential in a laterally bent NW by making the following assumptions: (i) piezoelectric equations were simplified using the perturbation theory, (ii) semiconducting effects were neglected and the NW was considered as cylindrical, (iii) elastic constants were taken isotropic, with Young modulus  $Y$  and Poisson ratio  $\nu$ , and (iv) the calculation was carried out in the limit of Saint-Venant's principle [4]. They showed that the piezoelectric charge density distribution within the NW yielded a piezopotential when bended with a force  $f_y$ . The maximum potential, located at the surface of the NW, was given by:

$$V_{max} = \pm \frac{f_y}{\pi Y} \frac{1}{(\epsilon_0 + \epsilon_1)} [e_{33} - 2(1 + \nu)e_{15} - 2\nu e_{31}] \frac{1}{R} \quad (3)$$

where  $R$  stands for NW radius and where the piezopotential is positive on the tensile side of the NW and negative on the compressive side (for a  $c^+$  axis orientation).  $\epsilon_0$  and  $\epsilon_1$  refer to vacuum permittivity and to ZnO relative permittivity normal to  $c$ -axis, respectively.

However the inverted region at the bottom of the NW cannot be predicted with the aforementioned analytical model.

Indeed, Saint-Venant's principle states that the calculated  $[T]$  is valid away from the areas where mechanical stresses are applied, i.e. far from load and from clamping. The inverted piezopotential region can be qualitatively explained by the reaction force created at the clamped end of the NW, which is opposite to the force applied at the free end. This discussion highlights the pertinence of FEM simulations for complex structures, which include the environment of the NW and complicated strain distributions with shear effects. This is mandatory to get a deeper insight in global pixel response, which is the key element in view of device design.

## III. RESULTS AND DISCUSSION

The evolution of the piezopotential generated in the NW ( $V_{NW}$ ) and of the output potential (i.e. the potential difference between the electrodes  $\Delta V_c$ ) were analyzed as a function of seed-layer thickness ( $e_{ZnO}$ ). We also evaluated the influence on pixel response of the gap  $\delta$  between electrodes and NW base, of electrodes thickness and of applied force.

### A. Influence of the seed-layer thickness

Fig. 2 maps the piezopotential distribution within a vertical section taken in the middle of a pixel when the NW is bent. This figure clearly demonstrates that the potential does not remain confined to the NW and that it extends from the inversion region into the seed-layer. The location of the maximum potential is indicated by point A and is located within the NW base. The potential in each electrode is constant. The output potential is taken at the electrode located on the compressed side of the NW, which will be referred to as point B in the following.

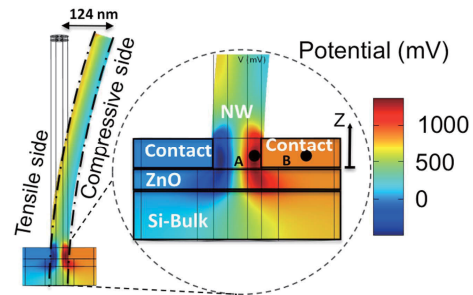


Fig. 2. Potential distribution in the pixel for  $e_{ZnO}=20$  nm. Maximum potential is observed at point A in the NW base. Output potential is measured within the floating electrode at point B.

Fig. 3a shows that  $V_{NW}$  and  $\Delta V_c$  are following similar trends (black lines, left axis). The piezopotential collection factor, or collection efficiency, can be estimated by the ratio  $V_{NW}/\Delta V_c$  (blue line, right axis). This ratio is larger for thinner layers, reaching up to 69 % for a 5 nm thick seed-layer. It drops down to 57 %, 50 % and 45 % for seed-layer thicknesses of 50 nm, 100 nm and 200 nm, respectively. In practice, these thicknesses can be standardly obtained by conventional deposition techniques, such as atomic layer deposition (ALD) or physical vapor deposition (PVD) techniques. It is important to keep in mind that even if thinner seed-layers are preferred,

the subsequently grown NW quality can be somehow affected, especially if polycrystalline textured layers are used [8].

Fig. 3b displays the potential profiles along the tensely and compressively stressed sides of the NW (along the dash-dot lines of Fig. 2) as a function of Z coordinate (with the origin taken at the NW base). The different plots show that piezopotential variations at the base of the NW are all following the same trend as seed-layer thickness varies. On tensile side, the piezopotential plateau at zero volts corresponds to the position of the grounded electrode and the lowest value is reached just below NW base. On compressive side, the plateau corresponds to the equipotential electrode region; the piezopotential reaches its maximal value at the interface between seed layer and NW and then decreases gradually towards the substrate.

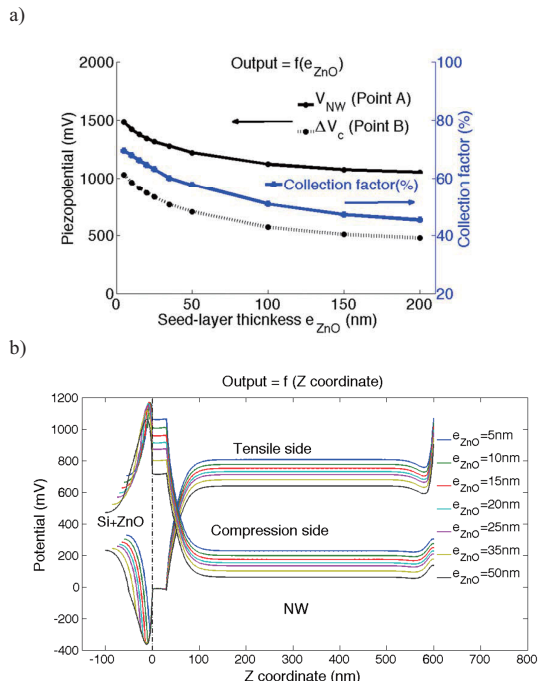


Fig. 3. a) Evolution of  $V_{NW}$  and  $\Delta V_c$  (black, full and broken lines, respectively, on the left axis) as function of the seed-layer thickness. The blue plot is the corresponding calculated potential collection factor (right axis), and b) potential profile along the tensely and compressively stressed sides of the NW for different seed-layer thicknesses.

### B. Influence of the NW-electrode contact quality

Microfabrication processes such as contact deposition or nanowire growth may induce some variability inherent to the fabrication flow. In order to investigate the issues related to effective contact between the electrodes and the NW base and their influence on the pixel response, we introduced a parameter  $\delta$ , corresponding to a possible gap between electrodes and NW. Here we illustrate the case where there are symmetrical gaps on both sides of the NW (Fig. 4a). The same calculations can naturally be carried out with one gap on a single side or with two gaps of different sizes (misalignment).

Fig. 4b maps the piezopotential in a section taken in the middle of the pixel. The extreme values were found at the interface between NW base and seed-layer. The results of the parametric analysis as a function of  $\delta$  are shown in Fig. 4c, for a seed-layer thickness fixed at 20 nm. At point A, an increase of piezopotential was first observed when  $\delta$  increased from 0 to the first simulated gap value (3 nm). This was explained by the changes in the stress-strain state at the NW base allowed by the loss of contact between metal electrodes and NW. However, once a gap was open, the value of  $V_{NW}$  remained quite stable.

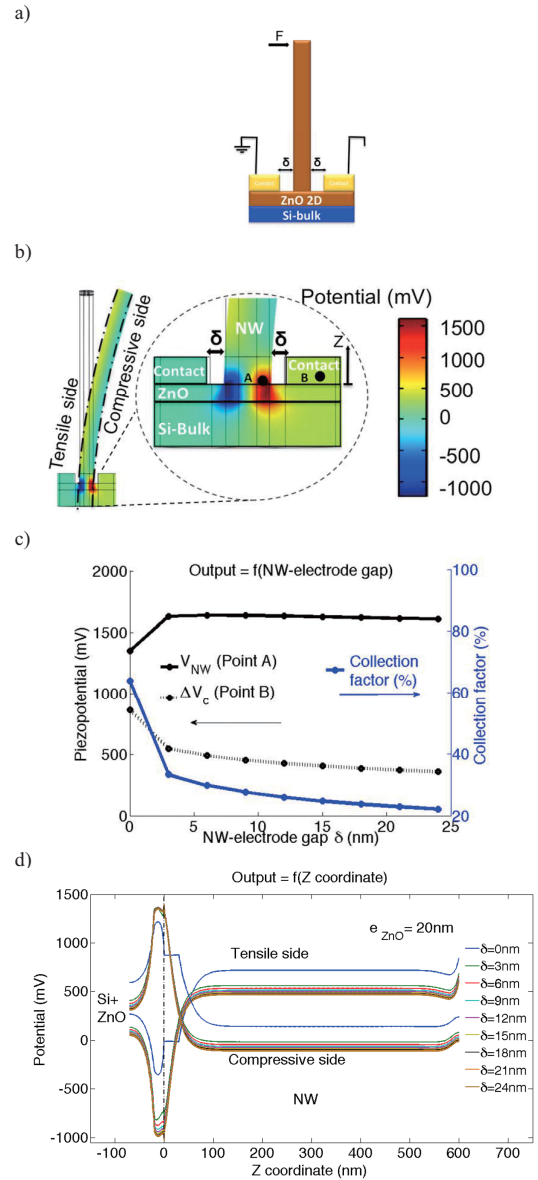


Fig. 4. a) Definition of parameter  $\delta$  in the device pixel, b) potential distribution in the pixel, c) evolution of the piezopotential in the NW and between the electrodes as a function of parameter  $\delta$  (for  $e_{ZnO}=20$  nm), and d) potential profile along the tensely and compressively stressed sides of the NW for different values of  $\delta$ .

Similarly,  $\Delta V_c$  fell down at gap opening and decreased more slowly afterwards (black, full and broken lines, left axis). For a 20 nm thick seed layer, the piezopotential collection factor was reduced from 60 % for  $\delta = 0$  nm to 33 % for  $\delta = 3$  nm, while tending to stabilize for larger values of  $\delta$  (blue line, right axis). Figure 4d shows the impact of gap opening on the potential profile on both tensile and compressive sides of the NW. For both profiles, no major variations were observed for  $\delta > 3$  nm.

### C. Influence of electrode thickness

The impact of the metallic electrode thickness  $h_{\text{contact}}$  on pixel response is illustrated in Fig. 5a and b with no gap and with a 18 nm gap, respectively. Two values of  $h_{\text{contact}}$ , 30 nm and 100 nm, were used for each value of  $\delta$ . Fig. 5 allows direct comparison of the four cases. On one hand, it was demonstrated that there was no influence of  $h_{\text{contact}}$  on pixel output for  $\delta > 0$  nm. On the other hand, for  $\delta = 0$  nm, the stress-strain state of the NW changed, resulting in a decrease in the generated piezopotential by about 10%.

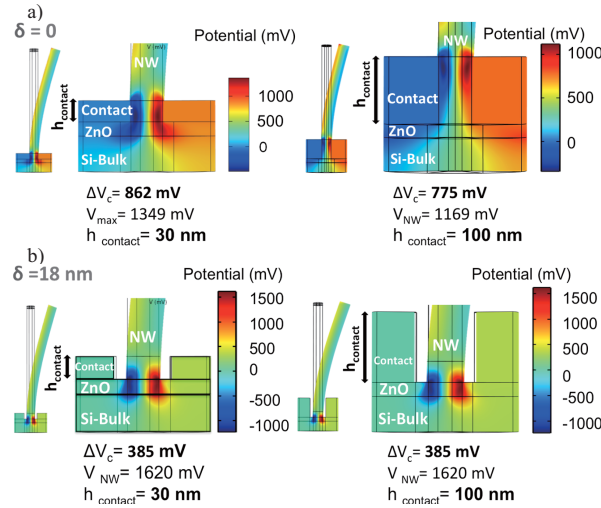


Fig. 5. Piezopotential mapping for two cases: a)  $\delta = 0$  nm and b)  $\delta = 18$  nm. Two values of  $h_{\text{contact}}$  (30 nm and 100 nm) are used in each case.

### D. Force dependence of the pixel response

Finally, the simulations were run with different values of the applied force  $F_y$  ranging from 10 nN to 80 nN with given values for  $h_{\text{contact}}$  (30 nm) and  $e_{\text{ZnO}}$  (20 nm), and two electrode configurations, with (i)  $\delta = 0$  nm, and (ii)  $\delta = 5$  nm. Fig. 6a and b show for both cases the piezopotential responses  $V_{\text{NW}}$  and  $\Delta V_c$  (black, full and broken lines, left axis) and the potential collection factor (blue line, right axis). The piezopotential was found to depend linearly on mechanical load in both cases, consistently with the linear assumption used for mechanical and piezoelectric properties. Potential collection factors were independent of input force and amounted to 60 % and 30 % for  $\delta$  equal to 0 nm and 5 nm, respectively.

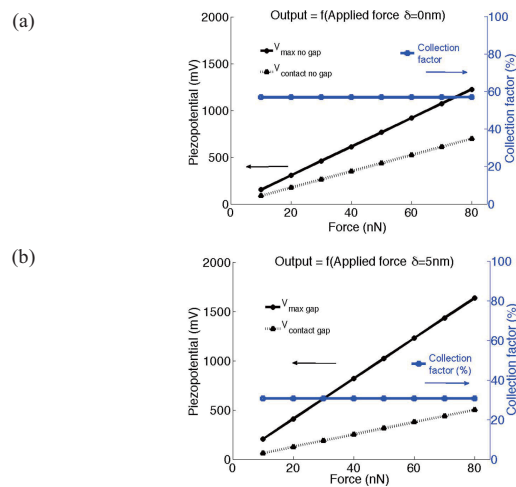


Fig. 6. Force-depending pixel response in the range 10 – 80 nN: a) case  $\delta = 0$  nm and b) case  $\delta = 18$  nm.

## IV. CONCLUSION

Our FEM simulations provided valuable insights for device design. Results can be summed up in 6 points: (i) the inverted region hosts the highest values of piezopotential: this is where the contacts should be placed; (ii) the piezopotential extends from the inversion region into the seed-layer; (iii) thinner seed-layers provide a larger pixel response; (iv) the pixel response drops significantly as soon as direct electrical contact with the NW is lost, and it falls to a value which is slowly decreasing with gap size and remains within exploitable range (tens and hundreds of mV); (v) the electrode thickness has little influence on pixel response; and (vi) piezopotential collection factor is independent of the force applied within the limits of linear elasticity and piezoelectricity. Microfabrication can be advantageously anticipated through such insights.

## ACKNOWLEDGMENT

Authors acknowledge support from PIEZOMAT EU Project No. 611019.

## REFERENCES

- [1] R. Agrawal, B. Peng, and H. D. Espinosa, "Experimental-computational Investigation of ZnO nanowires strength and fracture," *Nano Lett.*, vol. 9, no. 12, pp. 4177–4183, 2009.
- [2] Z. L. Wang, "Piezopotential gated nanowire devices: piezotronics and piezo-phototronics," *Nano Today*, vol. 5, no. 6, pp. 540–553, Dec. 2010.
- [3] R. Hinchet et al., "Scaling rules of piezoelectric nanowires in view of sensor and energy harvester integration," *Electron Devices Meeting (IEDM), IEEE International, 2012*, pp. 6.2.1–6.2.4.
- [4] Y. Gao and Z. L. Wang, "Electrostatic potential in a bent piezoelectric nanowire. The fundamental theory of nanogenerator and nanopiezotronics," *Nano Lett.*, vol. 7, no. 8, pp. 2499–2505, 2007.
- [5] C. Falconi, G. Mantini, A. D'Amico, and Z. L. Wang, "Studying piezoelectric nanowires and nanowalls for energy harvesting," *Sensors Actuators B Chem.*, vol. 139, no. 2, pp. 511–519, Jun. 2009.
- [6] Z.L. Wang, "Nano-piezotronics," *Adv. Mater.*, 19 (2007) 889-892.
- [7] L. D. Landau and E. M. Lifshitz, *Course of theoretical physics Vol 7: Theory of elasticity*. Elsevier Science & Technology Books, 1986.
- [8] R. Erdélyi et al., "Investigations into the impact of the template layer on ZnO nanowire arrays made using low temperature wet chemical growth," *Cryst. Growth Des.*, vol. 11, pp. 2515–2519, 2011.